

GeoPlanet: Earth and Planetary Sciences

Monika B. Kalinowska
Magdalena M. Mrokowska
Paweł M. Rowiński *Editors*

Recent Trends in Environmental Hydraulics

38th International School of Hydraulics

 Springer

GeoPlanet: Earth and Planetary Sciences

Editor-in-Chief

Paweł M. Rowiński , Institute of Geophysics, Polish Academy of Sciences,
Warsaw, Poland

Series Editors

Marek Banaszekiewicz, Warsaw, Poland

Janusz Pempkowiak, Sopot, Poland

Marek Lewandowski, Warsaw, Poland

Marek Sarna, Warsaw, Poland

The GeoPlanet series is a forum for presenting the latest achievements in the Earth and space sciences. It is published by the GeoPlanet consortium (Earth and Planetary Research Centre) formed by five institutes affiliated with the Polish Academy of Sciences: Institute of Geophysics, Space Research Centre, Institute of Geological Sciences, and Institute of Oceanology, and Nicolaus Copernicus Astronomical Centre. Its main objective is a multidisciplinary approach to link scientific activities in various Earth-related fields (geophysics, geology, oceanology) with Solar System research. Our publications encompass topical monographs and selected conference proceedings, authored or edited by leading experts of international repute as well as by promising young scientists. The GeoPlanet series aims to provide the stimulus for new ideas and discoveries by reporting on the state of the art and laying the foundations for the future development of the Geosciences.

More information about this series at <http://www.springer.com/series/8821>


Monika B. Kalinowska ·
Magdalena M. Mrokowska ·
Paweł M. Rowiński
Editors


Recent Trends in Environmental Hydraulics


38th International School of Hydraulics

 Springer

Editors

Monika B. Kalinowska 
Institute of Geophysics
Polish Academy of Sciences
Warsaw, Poland

Magdalena M. Mrokowska 
Institute of Geophysics
Polish Academy of Sciences
Warsaw, Poland

Paweł M. Rowiński 
Institute of Geophysics
Polish Academy of Sciences
Warsaw, Poland

The GeoPlanet: Earth and Planetary Sciences Book Series is in part a continuation of Monographic Volumes of Publications of the Institute of Geophysics, Polish Academy of Sciences, the journal published since 1962 (<http://pub.igf.edu.pl/index.php>).

ISSN 2190-5193 ISSN 2190-5207 (electronic)
GeoPlanet: Earth and Planetary Sciences
ISBN 978-3-030-37104-3 ISBN 978-3-030-37105-0 (eBook)
<https://doi.org/10.1007/978-3-030-37105-0>

© Springer Nature Switzerland AG 2020

This work is subject to copyright. All rights are reserved by the Publisher, whether the whole or part of the material is concerned, specifically the rights of translation, reprinting, reuse of illustrations, recitation, broadcasting, reproduction on microfilms or in any other physical way, and transmission or information storage and retrieval, electronic adaptation, computer software, or by similar or dissimilar methodology now known or hereafter developed.

The use of general descriptive names, registered names, trademarks, service marks, etc. in this publication does not imply, even in the absence of a specific statement, that such names are exempt from the relevant protective laws and regulations and therefore free for general use.

The publisher, the authors and the editors are safe to assume that the advice and information in this book are believed to be true and accurate at the date of publication. Neither the publisher nor the authors or the editors give a warranty, expressed or implied, with respect to the material contained herein or for any errors or omissions that may have been made. The publisher remains neutral with regard to jurisdictional claims in published maps and institutional affiliations.

This Springer imprint is published by the registered company Springer Nature Switzerland AG
The registered company address is: Gewerbestrasse 11, 6330 Cham, Switzerland

Series Editors

- Geophysics Paweł M. Rowiński
Editor-in-Chief
Institute of Geophysics
Polish Academy of Sciences
ul. Ks. Janusza 64
01-452 Warszawa, Poland
p.rowinski@igf.edu.pl
- Space Sciences Marek Banaszekiewicz
Space Research Centre
Polish Academy of Sciences
ul. Bartycka 18A
00-716 Warszawa, Poland
- Oceanology Janusz Pempkowiak
Institute of Oceanology
Polish Academy of Sciences
Powstańców Warszawy 55
81-712 Sopot, Poland
- Geology Marek Lewandowski
Institute of Geological Sciences
Polish Academy of Sciences
ul. Twarda 51/55
00-818 Warszawa, Poland
- Astronomy Marek Sarna
Nicolaus Copernicus Astronomical Centre
Polish Academy of Sciences
ul. Bartycka 18
00-716 Warszawa, Poland
sarna@camk.edu.pl

Managing Editor

Anna Dziembowska

Institute of Geophysics, Polish Academy of Sciences

Advisory Board

Robert Anczkiewicz

Research Centre in Kraków
Institute of Geological Sciences
Kraków, Poland

Aleksander Brzeziński

Space Research Centre
Polish Academy of Sciences
Warszawa, Poland

Javier Cuadros

Department of Mineralogy
Natural History Museum
London, UK

Jerzy Dera

Institute of Oceanology
Polish Academy of Sciences
Sopot, Poland

Evgeni Fedorovich

School of Meteorology
University of Oklahoma
Norman, USA

Wolfgang Franke

Geologisch-Paläntologisches Institut
Johann Wolfgang Goethe-Universität
Frankfurt/Main, Germany

Bertrand Fritz

Ecole et Observatoire des
Sciences de la Terre
Laboratoire d'Hydrologie
et de Géochimie de Strasbourg
Université de Strasbourg et CNRS
Strasbourg, France

Truls Johannessen

Geophysical Institute
University of Bergen
Bergen, Norway

Michael A. Kaminski

Department of Earth Sciences
University College London
London, UK

Andrzej Kijko

Aon Benfield
Natural Hazards Research Centre
University of Pretoria
Pretoria, South Africa

Francois Leblanc

Laboratoire Atmospheres, Milieux
Observations Spatiales, CNRS/IPSL
Paris, France

Kon-Kee Liu

Institute of Hydrological
and Oceanic Sciences
National Central University Jhongli
Jhongli, Taiwan

Teresa Madeyska

Research Centre in Warsaw
Institute of Geological Sciences
Warszawa, Poland

Antonio Meloni

Instituto Nazionale di Geofisica
Rome, Italy

Evangelos Papathanassiou

Hellenic Centre for Marine Research
Anavissos, Greece

Kaja Pietsch

AGH University of Science
and Technology
Kraków, Poland

Dušan Plašienka

Prírodovedecká fakulta, UK
Univerzita Komenského
Bratislava, Slovakia

Barbara Popielawska

Space Research Centre
Polish Academy of Sciences
Warszawa, Poland

Tilman Spohn

Deutsches Zentrum für Luftund
Raumfahrt in der Helmholtz
Gemeinschaft
Institut für Planetenforschung
Berlin, Germany

Krzysztof Stasiewicz

Swedish Institute of Space Physics
Uppsala, Sweden

Ewa Szuszkiewicz

Department of Astronomy
and Astrophysics
University of Szczecin
Szczecin, Poland

Roman Teisseyre

Department of Theoretical Geophysics
Institute of Geophysics
Polish Academy of Sciences
Warszawa, Poland

Jacek Tronczynski

Laboratory of Biogeochemistry
of Organic Contaminants
IFREMER DCN_BE
Nantes, France

Steve Wallis

School of the Built Environment
Heriot-Watt University
Riccarton, Edinburgh
Scotland, UK

Waclaw M. Zuberek

Department of Applied Geology
University of Silesia
Sosnowiec, Poland

Piotr Życki

Nicolaus Copernicus Astronomical
Centre
Polish Academy of Sciences
Warszawa, Poland

Preface

Sustainable development, even more—survival of human beings, strongly depends on aquatic ecosystems, which are exposed to human impacts as they, for example, ultimately receive all kinds of waste from agriculture, industrial and technological production. There is also much evidence of poor management of river systems, being the result of poor understanding of the processes that occur in river streams, particularly when flow–biota, flow–vegetation and geomorphic settings are taken into account. Despite huge progress in the field of environmental hydraulics in recent years, investigations on freshwater ecosystem functioning still require further research investments. The issues discussed in the present volume analyse some emerging trends in environmental hydraulics, hoping to contribute towards an improved understanding of the functioning of rivers and other aquatic systems. This book embraces studies carried out in the field, in laboratory flumes as well as computational investigations, often representing truly interdisciplinary research methodologies.

Together with the authors who contributed to these articles, we sincerely hope our readers will enjoy these papers, which are the result of the debate led during the 38th International School of Hydraulics. This school, a biannual affair, is traditionally held in Poland, this time in 21–24 May 2019 at the Dębowa Góra Hotel situated near Płock, at the picturesque lake surrounded by the forest greenery. This school has been attended by scholars from all over the world, from thirteen countries. All papers were presented during the school, thoroughly discussed there, and all of them were peer-reviewed prior to the school and if needed, also after the event. The invited speakers at the meeting were **Aronne Armanini** from University of Trento, Italy; **Alessandra Crosato** from IHE Delft Institute for Water Education, The Netherlands; **Subhasish Dey** Indian Institute of Technology Kharagpur, India; **Yafei Jia** from National Center for Computational Hydrosience and Engineering, The University of Mississippi, USA; **Juha Järvelä** from Aalto University, Finland;

Artur Magnuszewski from University of Warsaw, Poland; and **Wojciech Majewski** from Institute of Hydroengineering of Polish Academy of Sciences, Poland; world-class experts in the field and that guaranteed very high level of all the undertaking.

Warsaw, Poland

Monika B. Kalinowska
Paweł M. Rowiński
School Chairs

Acknowledgements

The editors are extremely grateful to all people who contributed to the organisation of the 38th International School of Hydraulics and the production of this volume.

We would like to express our thanks to all the authors for their contributions, and all the participants and speakers during the 38th International School of Hydraulics for sharing their knowledge and passion with others and engagement in all conference events.

The school and this book would not be possible without financial support from the Institute of Geophysics Polish Academy of Sciences statutory funds and Committee of Water Resources of the Polish Academy of Sciences. We want to express our thanks to the Institute of Geophysics Polish Academy of Sciences, CIFAL Płock, City Mayor of Płock and BMsonic company for being a sponsor of the prizes in the competition: “Best Young Researchers Presentation Award”. We were also glad to be able to run the conference under the auspices of International Association of Hydro-Environment Engineering and Research, as well as under the Honorary Patronage of the City Mayor of Płock. Very special thanks go to Artur Magnuszewski for his invaluable help in organising a study trip and also to the BMsonic—a Polish company for being with us during the conference and for organising an extraordinary event—a hot air tethered balloon flights during the conference.

We would like to express our cordial thanks to all the people from the local organising committee who helped make this conference a success. They are Hanna Baczyńska, Emilia Karamuz, Michael Nones and people from Mazurkas Congress and Conference Management company. We should also name Anna Dziembowska responsible for the high quality of English of the papers, and Karolina Branicka for all help while preparing the papers for this volume.

Finally, we wish to thank and acknowledge all the reviewers, who have donated their time and expertise to assist in improving the quality of the submitted papers:

- **Jochen Aberle**, Technical University Braunschweig, Germany
- **Mário J. Franca**, IHE Delft Institute for Water Education, The Netherlands
- **Ian Guymer**, The University of Sheffield, UK

- **Monika B. Kalinowska**, Institute of Geophysics, Polish Academy of Sciences, Poland
- **Emilia Karamuz**, Institute of Geophysics, Polish Academy of Sciences, Poland
- **Leszek Książek**, The University of Agriculture in Krakow, Poland
- **Bartłomiej Luks**, Institute of Geophysics, Polish Academy of Sciences, Poland
- **J. Russell Manson**, The Richard Stockton College of New Jersey, USA
- **Andrea Marion**, University of Padova, Italy
- **Magdalena M. Mrokowska**, Institute of Geophysics, Polish Academy of Sciences, Poland
- **Jarosław Napiórkowski**, Institute of Geophysics, Polish Academy of Sciences, Poland
- **Michael Nones**, Institute of Geophysics, Polish Academy of Sciences, Poland
- **Tomasz Okruszko**, Warsaw University of Life Sciences, Poland
- **Marzena Osuch**, Institute of Geophysics, Polish Academy of Sciences, Poland
- **Artur Radecki-Pawlik**, Cracow University of Technology, Poland
- **Renata Romanowicz**, Institute of Geophysics, Polish Academy of Sciences, Poland
- **Paweł M. Rowiński**, Institute of Geophysics, Polish Academy of Sciences, Poland
- **Michał Szydłowski**, Gdansk University of Technology, Poland
- **Steve Wallis**, Heriot-Watt University, UK
- **Kaisa Västilä**, Aalto University School of Engineering, Finland

Monika B. Kalinowska
Magdalena M. Mrokowska
Paweł M. Rowiński

Contents

| | |
|---|----|
| Turbulent Length Scales and Reynolds Stress Anisotropy in Wall-Wake Flow Downstream of an Isolated Dunal Bedform | 1 |
| Subhasish Dey and Sankar Sarkar | |
| A Free-Surface Immersed-Boundary Lattice Boltzmann Method for Flows in Porous Media | 23 |
| Ayurzana Badarch, John D. Fenton and Hosoyamada Tokuzo | |
| Modelling River Flow Through In-Stream Natural Vegetation for a Gravel-Bed River Reach | 33 |
| Simon D. A. Clark, James R. Cooper, Ponnambalam Rameshwaran, Pamela Naden, Ming Li and Janet Hooke | |
| On the Use of Surface PIV for the Characterization of Wake Area in Flows Through Emergent Vegetation | 43 |
| J. Leonardo Corredor-Garcia, Alexandre Delalande, Virginia Stovin and Ian Guymer | |
| Dominant Hydraulic Conditions in the 2-D Model—Vistula River from Zawichost to Słupia Nadbrzeżna | 53 |
| Jacek Florek, Maciej Wyrębek and Agnieszka Woś | |
| Water Level Uncertainties Due to Uncertain Bedform Dynamics in the Dutch Rhine System | 67 |
| Matthijs R. A. Gensen, Jord J. Warmink and Suzanne J. M. H. Hulscher | |
| Discharge Characteristics of Triangular Weir with Upstream Ramp and Its CFD Modelling Using Ansys CFX Module | 77 |
| Subhojit Kadia, Binit Kumar and Zulfequar Ahmad | |
| Modelling of Velocity Distribution in a Channel Partly Covered by Submerged Vegetation | 91 |
| Monika B. Kalinowska, Kaisa Västilä, Adam Koziół, Paweł M. Rowiński, Adam Kiczko and Janusz Kubrak | |

| | |
|---|-----|
| Habitat Structure Changes of the Wisloka River as a Result of Channel Restoration | 103 |
| Leszek Książek, Agnieszka Woś, Maciej Wyrębek and Andrzej Strużyński | |
| Theoretical Analysis of the Reduction of Pressure Wave Velocity by Internal Circular Tubes | 117 |
| Michał Kubrak and Apoloniusz Kodura | |
| An Experimental Investigation of Reaeration and Energy Dissipation in Hydraulic Jump | 127 |
| Serhat Kucukali and Sevket Cokgor | |
| Flow and Turbulence Structure in a Vertical Slot–Brush Fish Pass | 137 |
| Serhat Kucukali and Reinhard Hassinger | |
| Flow Between the Sub-basins of Charzykowskie Lake—Modeling and Measurements | 147 |
| Artur Magnuszewski and Barbara Nowicka | |
| LIDAR Data Application in the Process of Developing a Hydrodynamic Flow Model Exemplified by the Warta River Reach | 159 |
| Albert Malinger, Tomasz Kałuża and Tomasz Dysarz | |
| On Habitat Complexity in Streams Derived from the Analysis of Tracer Data | 171 |
| J. Russell Manson, Steve G. Wallis, Artur Radecki-Pawlik, Karol Plesinski and Peggy Zinke | |
| Quantification of Flood Hazards Due to Assumed Breaching of Attabad Landslide Dam, Pakistan | 181 |
| Arham Mansoor, Noor Muhammad Khan, Aziz Akbar, Yasir Abbas and Muhammad Umar Farooq | |
| Monitoring of Riparian Vegetation Growth on Fluvial Sandbars | 197 |
| Michael Nones, Massimo Guerrero and Renata Archetti | |
| Hydrodynamics of Water-Worked and Screeded Gravel-Bed Flows | 207 |
| Ellora Padhi, Nadia Penna, Subhasish Dey and Roberto Gaudio | |
| Quantitative Characterization of the Roughness of Four Artificially Prepared Gravel Surfaces | 219 |
| Jie Qin, Teng Wu and Deyu Zhong | |
| Rosette Diffuser for Dense Effluent—Puck Bay Case Study | 231 |
| Małgorzata Robakiewicz | |
| Turbulence in Wall-Wake Flow Downstream of an Isolated Dune | 241 |
| Sankar Sarkar and Subhasish Dey | |

Automatic Calibration of a 3D Morphodynamic Numerical Model for Simulating Bed Changes in a 180° Channel Bend 253
Vahid Shoarinezhad, Silke Wieprecht and Stefan Haun

Sand Island Reshaping in Response to Selected Discharges: The Vistula River Returning to Its Natural State 263
Andrzej Strużyński, Maciej Wyrębek, Adam Nowak, Agnieszka Woś, Jacek Florek and Leszek Książek

Shallow Water Equations as a Mathematical Model of Whitewater Course Hydrodynamics 277
Michał Szydłowski and Patrycja Mikos-Studnicka

Velocity Distribution and Dip Phenomenon in a Large Amplitude Meandering Channel 289
Donatella Termini

Numerical Modeling of Extreme Flooding for Flood Risk Assessment in the Tra Bong River Basin, Vietnam 299
Xuan Manh Trinh and Frank Molkenhain

Application of the STIR Model to a Small River at Different River Flow Rates 309
Steve G. Wallis and Eleonora Dallan

Turbulent Length Scales and Reynolds Stress Anisotropy in Wall-Wake Flow Downstream of an Isolated Dunal Bedform



Subhasish Dey and Sankar Sarkar

Abstract This experimental study brings the turbulent length scales and the Reynolds stress anisotropy into focus in wall-wake flow downstream of an isolated dunal bedform. The results reveal that wall-wake flow downstream of an isolated dune possesses a high-turbulence level having its peak value at the dune crest level. This level lasts up to the vertical distance until the effects of the dune on the flow disappears. Regarding the turbulent length scales, downstream of the dune, the Prandtl's mixing length in wall-wake flow is greater than that in undisturbed upstream flow, while the Taylor microscale and the Kolmogorov length scale are smaller. In Reynolds stress anisotropy analysis, the anisotropy invariant maps demonstrate the data plots form a looping trend in wall-wake flow. Below the dune crest, the turbulence is characterized with an affinity to show a two-dimensional isotropy, while above the crest, the anisotropy has a tendency to reduce to a quasi-three-dimensional isotropy.

Keywords Dune · Turbulent flow · Open-channel flow · Turbulent length scales · Reynolds stress anisotropy

1 Introduction

Natural turbulent streams often come across bed-mounted solid obstacles of different geometries that play an important role in modifying flow characteristics. These obstacles are often called *bluff-bodies* in applied hydrodynamics. The presence of a bed-mounted bluff-body in a streamflow generates wakes at its downstream, called the *wall-wake flow*. Depending on the geometry of a bluff-body and the magnitude of streamflow velocity, the wake flow downstream of the bluff-body sustains up to a

S. Dey (✉)

Department of Civil Engineering, Indian Institute of Technology Kharagpur, Kharagpur, West Bengal 721302, India
e-mail: sdey@iitkgp.ac.in

S. Sarkar

Physics and Applied Mathematics Unit, Indian Statistical Institute, Kolkata, West Bengal 700108, India

© Springer Nature Switzerland AG 2020

M. B. Kalinowska et al. (eds.), *Recent Trends in Environmental Hydraulics*, GeoPlanet: Earth and Planetary Sciences,
https://doi.org/10.1007/978-3-030-37105-0_1

certain distance until the undisturbed upstream velocity profile is eventually recovered. Owing to the importance of bluff-bodies in practical purposes, the wake flow downstream of a bluff-body remains a topic of immense importance in applied hydrodynamics (Bose and Dey 2016, 2018). Schlichting (1979) was the pioneer to study the wall-wake flow downstream of a circular cylinder developed by the approach shear-free flow, providing a similarity theory for the velocity defect profile in the free wake flow. However, the wall-wake flow downstream of a bed-mounted obstacle under an approach wall-shear flow is more complex being different from the free wake flow. Limited studies have been carried out to understand the turbulence characteristics downstream of bed-mounted bluff-bodies in both near- and far-wake under a shear flow. To be specific, Balachandar et al. (2000) and Tachie and Balachandar (2001) argued that the similarity for velocity profiles in the wall-wake downstream of a bed-mounted plate could be preserved even in the near-wake flow zone by using the appropriate velocity and length scales. Shamloo et al. (2001) studied the effects of hemispherical objects in characterizing the streamwise velocity and Reynolds shear stress in an open-channel flow. Downstream of a hemisphere, they observed a recirculation zone, which disappeared after a downstream distance of about twice the hemisphere diameter. Kahraman et al. (2002) observed that the effects of localized wall-roughness on shallow wake flow downstream of a bed-mounted circular cylinder are not only confined to the near-wall flow zone, but also govern the entire turbulence in a shallow wake flow covering up to the half of the flow depth. Some researchers were also interested to study the vortex shedding in wall-wake flows. Akilli and Rockwell (2002), Ozturk et al. (2008) and Ozgoren (2006) studied the near-wake flow downstream of a bed-mounted vertical circular cylinder by particle image velocimetry (PIV). Akilli and Rockwell (2002) observed that a large-scale Kármán vortex that contains upward ejections through its core is developed and ultimately becomes a streamwise vortex, inducing a distortion to the free surface. Ozturk et al. (2008) studied the flow field upstream and downstream of a bed-mounted vertical circular cylinder within the boundary layer involving the interaction among the primary and the trail of the horseshoe vortices developed at the upstream cylinder base. On the other hand, Ozgoren (2006) studied the generation of vortical structures and the turbulence quantities downstream of a bed-mounted vertical circular cylinder under a uniform flow. They reported that the length of vortex formation decreases as the Reynolds number increases. Lacey and Roy (2008) studied the turbulent flow downstream of a submerged pebble cluster and observed a dominance of longitudinal-vertical vortex shedding in the wake of the cluster. Sadeque et al. (2009) considered the bed-mounted cylinders as bluff-bodies and found that the flow far from the bed is approximately similar and can be described by the plane wake flow equation. Further progresses in understanding the wake flow characteristics downstream of bluff-bodies have been recently made by Dey et al. (2011, 2018a, b, c), Sarkar and Dey (2015a, b).

Considering an isolated dunal bedform as a bluff-body and studying the flow characteristics downstream of it, inadequate attention has so far been paid to the best of the authors' knowledge. Importantly, the existing knowledge of flow over an isolated dune is not sufficient in predicting the flow over it, because most of the cases

were studied for the flow over a series of dunes. For instance, McLean and Smith (1986) and Nelson and Smith (1989) studied the turbulent flow field over the dunes and observed the existence of separation zone, reattachment point, wake flow zone, internal boundary layer, etc. Maddux et al. (2003a, b), who experimentally studied the turbulent flow over a series of two- and three-dimensional dunes observed that the three-dimensional dunes possess different turbulence characteristics from the two-dimensional ones. Based on the laboratory experiments, Best (2005) showed that the ejections dominate the instantaneous flow field over the crests of the dunes and the highest instantaneous Reynolds stresses are associated with the ejections and sweeps.

It is evident from the recent studies by Sarkar and Dey (2015a, b), and Dey et al. (2018b) that the bluff-bodies have significant impacts on the eddy sizes and the turbulence anisotropy. To be specific, the turbulent flow contains large number of eddies, which can be described by their traversing distances by using Prandtl's mixing length and their sizes by using the Taylor microscale and the Kolmogorov length scale. In addition, the characterization of turbulent flow requires an understanding of anisotropy as it provides information on the extent of departure from the isotropy (Lumley and Newman 1977; Smalley et al. 2002; Keirsbulck et al. 2002; Dey et al. 2019). However, a few studies have been reported to understand the turbulent length scales and Reynolds shear stress anisotropy for the case of an isolated dune. This study is therefore dedicated to characterize the turbulent length scales and the Reynolds stress anisotropy in the flow downstream of an isolated dunal bedform mounted on a rough bed.

2 Experimental Setup

Experiments were carried out in a re-circulatory rectangular flume of 20 m length, 0.5 m width and 0.5 m depth at the Fluvial Mechanics Laboratory in the Indian Statistical Institute, Kolkata, India. The flume was facilitated with visual observation of flow through its transparent sidewalls. A centrifugal pump was used to supply the inflow discharge, which was measured by an electromagnetic device.

The flume bed that had a bed slope of 0.03% was created rough by gluing gravels. Uniform gravels of a median size of $d_{50} = 2.49$ mm were used for this purpose. Isolated two-dimensional dunal (triangular) bedforms for Runs 1 and 2, as shown in Fig. 1, were mounted on the bed at a distance of 7 m from the flume inlet. A dune is of scalene triangular shape with its length l as the horizontal length of the triangular base summing the lengths of stoss-side l_S and leeside l_L , given by $l = l_S + l_L$ (Fig. 2). The dune height h_d is the vertical distance of the dune crest from the bed. The dune was also made rough by using the same gravel sample. Two dunes were used with height $h_d = 0.09$ m and length $l (= l_S + l_L = 0.24 + 0.16) = 0.4$ m for Run 1 and $h_d = 0.03$ m and $l (= l_S + l_L = 0.24 + 0.06) = 0.3$ m for Run 2. Both the runs were performed under the same approach uniform flow condition with a flow depth of $h \approx 0.3$ m and the depth-averaged approach velocity of $\bar{U} \approx$

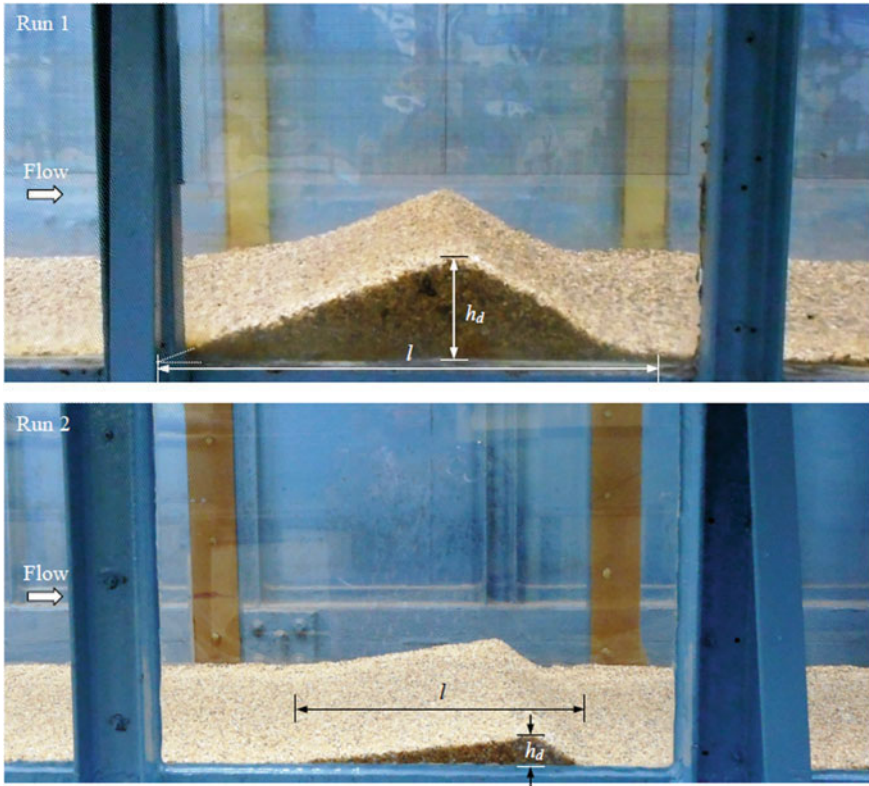


Fig. 1 Photographs of bed-mounted isolated dunal bedforms in the experimental flume

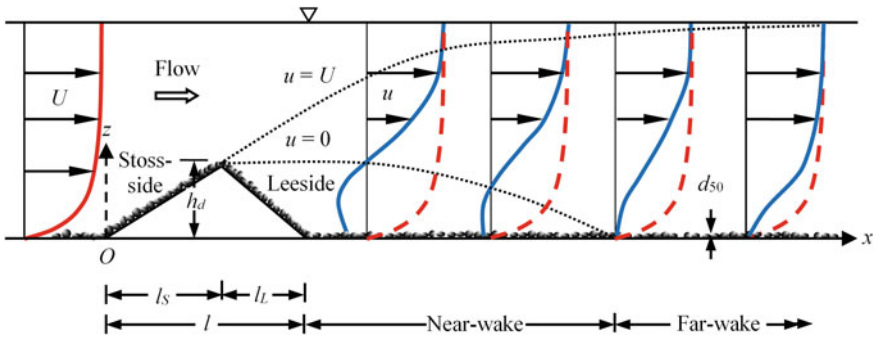


Fig. 2 Schematic of an isolated dunal bedform and velocity profiles

0.44 m s^{-1} . In both Runs, 1 and 2, the flow depth and approach velocity were slightly different (about 1.5%) owing to the experimental rearrangements. A Vernier point gauge with a precision of $\pm 0.1 \text{ mm}$ was used to measure the flow depth and the free surface profile. The approach shear velocity u_* , calculated from the bed slope, was $0.030 \text{ (m s}^{-1}\text{)}$, while the values of u_* for Runs 1 and 2, obtained from the Reynolds shear stress profiles, were 0.027 and 0.025 m s^{-1} , respectively. The flow Reynolds number and Froude number were $528,000$ and 0.256 , respectively, for both the runs. Besides, the shear-particle Reynolds number $R_* (= d_{50}u_*/\nu$, where ν is the coefficient of kinematic viscosity of water) was $74.7 (>70)$ for both the runs, ensuring the flow to be turbulent-rough and subcritical. The instantaneous velocities were measured along the centerline of the flume at different nondimensional streamwise locations (according to the coordinate system shown in Fig. 2) $x/l = -0.5, -0.25, 0, 0.1, 0.2, 0.3, 0.4, 0.5, 0.6, 0.7, 0.8, 0.9, 1, 1.1, 1.3, 1.7, 2.1, 2.5,$ and 3.3 by using a 5 cm downlooking *Vecrtino velocimeter*. Here, x is the streamwise distance. The Vecrtino system had an adjustable sampling volume of 6 mm diameter and $1\text{--}4 \text{ mm}$ height. It was operated with an acoustic frequency of 10 MHz and at a sampling rate of 100 Hz . The velocity components u , v , and w were considered in the streamwise (x), spanwise (y), and vertical (z) directions, respectively. Up to the dune crest, the lowest sampling height of 1 mm was used, while above the crest, it was set as 2.5 mm . A sampling duration of 300 s was considered to be sufficient to get the time-invariant velocity and turbulence quantities. The minimum signal-to-noise ratio (SNR) and signal correlation were maintained as 18 and 70% , respectively. After the measurements, the data were filtered whenever necessary using the *acceleration thresholding method* (Goring and Nikora 2002).

3 Time-Averaged Velocity, Reynolds Shear Stress and Average Turbulence Intensity

Figure 2 presents a schematic of an isolated dunal bedform and the velocity profiles upstream and downstream of it. The flow is directed from the stoss-side to the leeside. Therefore, the approach flow before starting the stoss-side of the dune is designated herein as upstream flow and the flow past the dune as wall-wake flow. Immediate downstream vicinity of the dune ($x = \xi l$, where ξ is a factor being less than unity), the flow is characterized by the reversed flow, called the *near-wake flow*. Thereafter, the flow is called the *far-wake flow*. In Fig. 2, the upper dotted line represents the boundary layer ($u = U$) in wall-wake flow and the lower dotted line signifies the locus of $u = 0$, where $u(z)$ is the streamwise velocity in wake flow, $U(z)$ is the streamwise velocity in undisturbed upstream flow and z is the vertical distance measured from the bed. The far-wake flow having a defect velocity profiles starts recovering, as the flow travels downstream. Far downstream of the dune, the flow fully recovers the undisturbed upstream flow, signifying the fully recovered (or fully developed) open-channel flow.

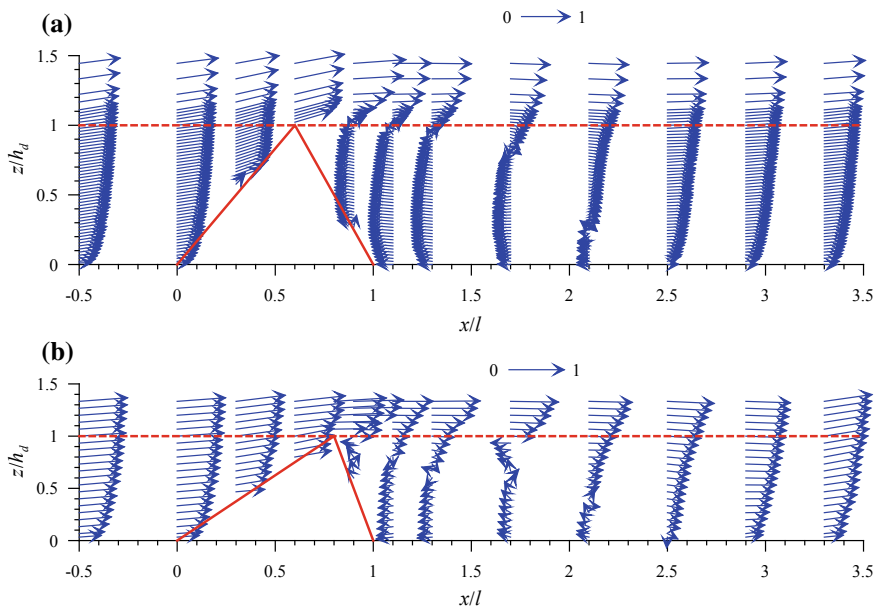


Fig. 3 Velocity vectors in flows upstream and downstream of an isolated dune in **a** Run 1 and **b** Run 2 (dune geometries not to in same horizontal and vertical scales)

The time-averaged velocity vectors for Runs 1 and 2 are depicted in Fig. 3a, b, respectively, where the abscissa and the ordinate represent the nondimensional streamwise distance x/l and vertical distance z/h_d , respectively. The magnitude and the direction of the velocity vectors are $(u^2 + w^2)^{0.5}$ and $\tan^{-1}(w/u)$, respectively, where u and w are the time-averaged streamwise and vertical velocities, respectively. Upstream of the dune ($x/l = -0.5$), the velocity vectors do not change significantly in magnitude and direction while approaching from $x/l = -0.5$ to 0 (starting point of the stoss-side of dune). However, downstream of the dune, the velocity vectors change significantly both in magnitude and direction, particularly below the dune crest. Immediate downstream vicinity of the dune ($1 \leq x/l \leq 1.75$), the velocity vectors change their directions, signifying a circulatory motion in the near-wake flow zone. The near-bed velocity vectors in the reverse direction continue up to a certain distance ($x/l \approx 1.75$) in the near-wake flow zone. However, the wall-wake flows in both the runs start recovering their respective undisturbed upstream flows with an increase in horizontal distance x/l , attaining approximately the undisturbed velocity vectors at $x/l = 3.3$ (or $x/h_d = 15$ and 33 in Runs 1 and 2, respectively).

Figure 4 shows the nondimensional streamwise velocity u/u_* profiles in flows upstream and downstream of an isolated dune at different streamwise distances for Runs 1 and 2. It is evident that the approach shear flow passing the isolated dune gets separated to form a reversed flow, in the near-wake flow zone, at the immediate downstream vicinity of the dune ($1 \leq x/l \leq 1.75$). As the flow moves further

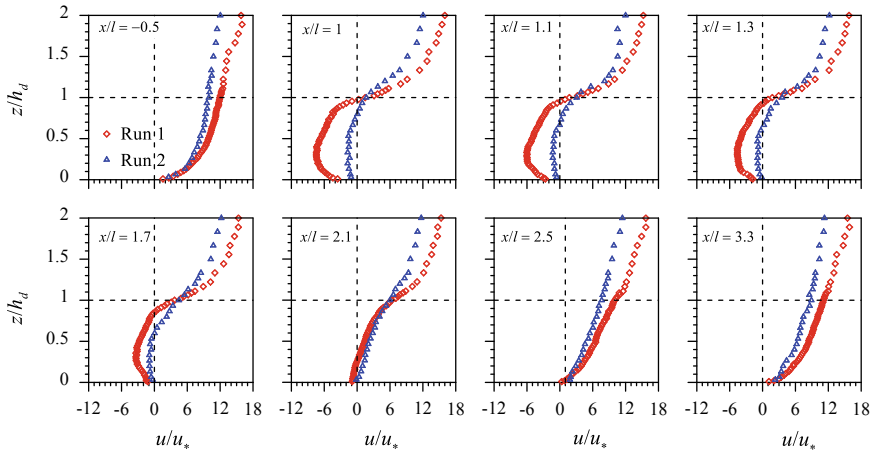


Fig. 4 Vertical profiles of nondimensional streamwise velocity u/u_* at different streamwise distances for Runs 1 and 2

downstream, the reversed flow disappears establishing the far-wake flow ($1.75 < x/l < 3.3$). Far downstream of the dune ($x/l \geq 3.3$), the velocity profiles in Runs 1 and 2 recover their respective undisturbed upstream profiles, called the *no-wake flow* or *fully recovered flow* (Sforza and Mons 1970; Sadeque et al. 2009; Dey et al. 2011). The main feature of u/u_* profiles in wall-wake flow is that the velocity gradient, which is milder and concave below the crest level, changes (forming an inflection point) at the crest level to become steeper and convex above it. However, the length of wall-wake flow zone and the distance of recovery of streamwise velocity profile for an isolated dune are different as compared to those for bed-mounted spherical obstacles (Dey et al. 2011) and bed-mounted horizontal and vertical cylinders (Dey et al. 2018a, b, c). The recovery of the streamwise velocity took place at a distance of 8.5 times the sphere diameter in Dey et al. (2011), while it was at a distance of 20 times the horizontal cylinder diameter in Dey et al. (2018a) and 16 times the vertical cylinder diameter in Dey et al. (2018b, c). In the present case, the recovery of the velocity profiles occurred approximately at 3.3 times the dune length or 15 and 33 times the dune height in Runs 1 and 2, respectively. The differences of the downstream locations to recover the undisturbed upstream streamwise velocity profiles in Runs 1 and 2 are attributed to the different geometries of the dunes.

Figure 5 displays the vertical profiles of nondimensional Reynolds shear stress (RSS) τ/u_*^2 in flows upstream and downstream of an isolated dune at different streamwise distances for Runs 1 and 2. Here, τ is the Reynolds shear stress relative to mass density ρ of water, defined by $-\overline{u'w'}$. Upstream of the dune ($x/l = -0.5$), the τ/u_*^2 profiles in both the runs follow approximately a linear law, where the peak values in τ/u_*^2 profiles appear in near the bed, decreasing linearly with an increase in vertical distance and approaching to zero at the free surface. However, downstream of the dune, the τ/u_*^2 profiles start with a finite value from the bed and increase with an

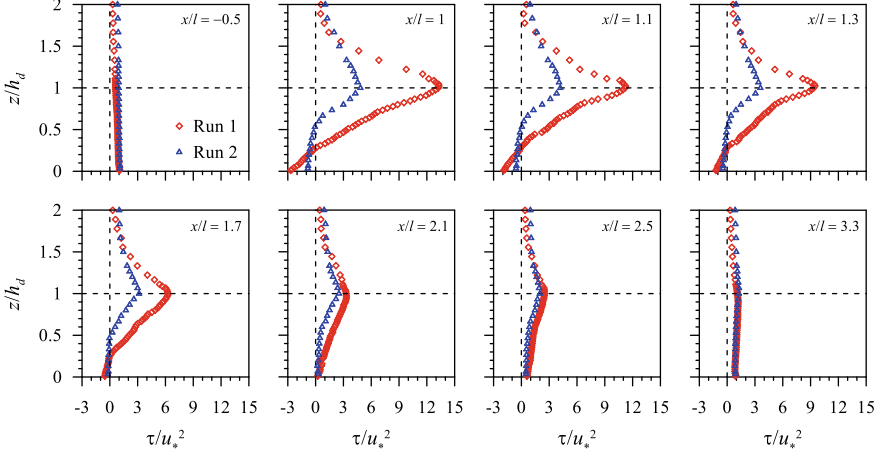


Fig. 5 Vertical profiles of nondimensional Reynolds shear stress τ/u_*^2 at different streamwise distances for Runs 1 and 2

increase in vertical distance until they attain their peaks at the dune crest. Then, they decrease, as one goes toward the free surface. The peaks in τ/u_*^2 profiles progressively diminish with an increase in downstream distance. However, far downstream of the dune ($x/l = 3.3$), the τ/u_*^2 profiles in both the runs follow the undisturbed upstream profiles of the respective runs, confirming a stress recovery. It can be concluded that at a given vertical distance, the RSS in wall-wake flow is greater than that in undisturbed upstream flow owing to the fluid mixing in wall-wake flow zone.

The vertical profiles of average turbulence intensity I_{av} at different streamwise distances for Runs 1 and 2 are shown in Fig. 6. The average turbulence intensity I_{av} is used to assess the overall turbulence level. It is expressed as $I_{av} = (2q/3)^{0.5}/U_1$; where q is the turbulent kinetic energy (TKE) [$= 0.5(u'u' + v'v' + w'w')$], $u'u'$, $v'v'$, and $w'w'$ are the Reynolds normal stresses relative to ρ in streamwise, spanwise and vertical directions, respectively, and U_1 is the local time-averaged resultant velocity [$= (u^2 + v^2 + w^2)^{0.5}$]. In case of a pipe flow, the ranges $I_{av} = 0.05$ – 0.2 , 0.01 – 0.05 and <0.01 represent the high-turbulence, medium-turbulence and low turbulence, respectively (Russo and Basse 2016; Basse 2017). However, these ranges are deemed to be applicable to the turbulent flow in an open channel as well.

The vertical profiles of I_{av} at different streamwise distances show that upstream of the dune ($x/l = -0.5$), the I_{av} starts with a bed induced high-turbulence level from the near bed, but as the vertical distance increases, the I_{av} profiles gradually reduces to medium and then to low turbulence range. However, downstream of the dune, the I_{av} profiles start with a high-turbulence level close to the bed, but after a brief decrease, the I_{av} profiles increase sharply with vertical distance, attaining their peak values at the dune crest. It indicates the maximum value in high-turbulence level owing to an intense fluid mixing. Above the crest, the I_{av} profiles decrease with an increase in vertical distance and above $z/h_d = 1.5$, the I_{av} profiles fall sharply to

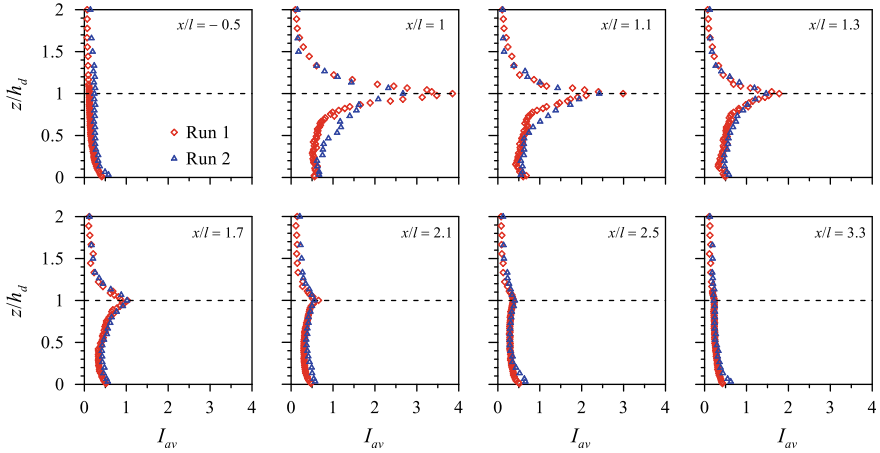


Fig. 6 Vertical profiles of average turbulence intensity I_{av} at different streamwise distances for Runs 1 and 2

follow the upstream profiles of respective runs. Importantly, the peaks of I_{av} taking place at the dune crest give an indication of the occurrence of the maximum TKE at the crest. The present findings are in conformity with the observations of Sarkar et al. (2016), who also found that the maximum TKE occurs at the crests of the protruding array of large gravels owing to the fluid mixing at the crest. In essence, the wall-wake flow possesses a high-turbulence level having a peak at the crest level indicating an intense fluid mixing. The high-turbulence level continues up to the vertical distance of 1.5 times the dune height, and beyond that the effects of the dune vanish.

4 Turbulent Length Scales

The turbulent fluid flow comprises the eddies that are dynamically self-perpetuate, as the fluid flows. The eddies collapse unremittingly from the largest scale to the smallest one, initiating from the intrinsic flow instabilities (Pope 2000). While the size and the travelling space of individual eddies are hard to determine uniquely, it is however feasible to delineate the length scales by characterizing the behavior of eddies. Remarkably, Prandtl (1925) was the innovator of the mixing-length concept that elucidates the mixing phenomenon by the turbulent eddies in a fluid flow stemming from the fluid momentum interchange in a macro-scale. The Prandtl's mixing-length thus indicates the travelling space of eddies. On the other hand, the turbulent length scale is a physical quantity to describe the behavior of the large energy-containing eddies in a turbulent flow. The large eddies in the flow account for most of the transport of momentum and energy. If a larger eddy collapses, its kinetic energy is transmitted to the smaller eddies in an energy cascade process. By contrast, when small eddies merge, as they often do in a mixing process, the TKE is

transmitted to the larger eddies. The length scale of larger eddies is controlled by the physical boundaries of a flow, while the length scale of smaller eddies can be defined by the TKE dissipation rate and the kinematic viscosity of fluid in terms of the *Taylor microscale* and the *Kolmogorov length scale*. The former refers to the length scale in the inertial subrange and the latter to the dissipation range (Pope 2000; Jovanović 2004; Dey 2014).

4.1 Prandtl's Mixing Length

Prandtl (1925) argued that in a turbulent shear flow, the eddies forming the fluid parcels generate and then degenerate to exchange their momentum after travelling an average distance, termed the *mixing length* (also well-known as *Prandtl's mixing length*). The process of generation and degeneration of eddies perpetuates as long as the fluid flows at a high Reynolds number. According to the Prandtl's mixing-length theory, the mixing-length l_p is expressed as

$$l_p(z) = \frac{(-\overline{u'w'})^{0.5}}{d\bar{u}/dz} \quad (1)$$

The nondimensional Prandtl's mixing-length l_p/d_{50} as a function of nondimensional vertical distance z/h_d at different nondimensional streamwise distances x/l for Runs 1 and 2 is plotted in Fig. 7. Upstream of the dune ($x/l = -0.5$), the l_p/d_{50} profiles increase almost linearly with an increase in vertical distance obeying $l_p = \kappa z$, where κ is the von Kármán constant (≈ 0.4). Downstream of the dune ($x/l \geq 1$), the l_p/d_{50}

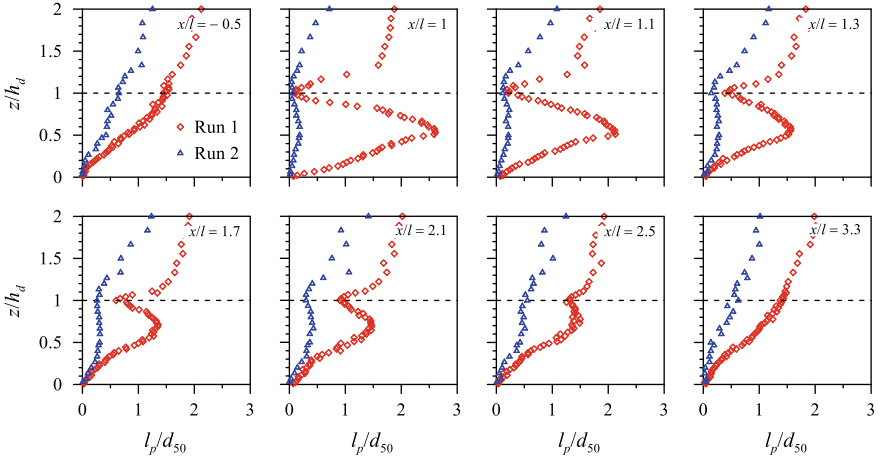


Fig. 7 Vertical profiles of nondimensional Prandtl's mixing length l_p/d_{50} at different streamwise distances for Runs 1 and 2

profiles increase sharply with an increase in vertical distance, attaining their peak values at $z/h_d \approx 0.5-0.6$. Then, they decrease to a second lowest critical value at the dune crest ($z/h_d \approx 1$) and, thereafter, gradually increase, as one goes toward the free surface. It is clearly noticeable that at a given z , the mixing-length l_p in wall-wake flow is greater than that in undisturbed upstream flow. The increased values of l_p/d_{50} gradually disappear with an increase in downstream distance. Far downstream of the dune ($x/l = 3.3$), the l_p/d_{50} profiles in both the runs become almost similar to their corresponding undisturbed upstream profiles displaying a recovery of mixing-length. It can be concluded that at a given vertical distance, the average travelling distance of turbulent eddies in wall-wake flow is greater than that in the undisturbed upstream flow. The reason is accredited to an increased RSS and a reduced velocity gradient in wall-wake flow.

4.2 Taylor Microscale

The Taylor microscale λ represents the eddy size in the inertial subrange of the Kolmogorov spectrum of velocity fluctuations being the pertinent length scale of the pure turbulence. It is expressed as

$$\lambda = \left(\frac{15\nu\sigma_u}{\varepsilon} \right)^{0.5} \quad (2)$$

where σ_u is the streamwise Reynolds normal stress relative to ρ , given by $\overline{u'u'}$, and ε is the TKE dissipation rate. In this study, the ε was estimated from the Kolmogorov second hypothesis, as was done by Dey and Das (2012).

The vertical profiles of nondimensional Taylor microscale λ/d_{50} at different nondimensional streamwise distances x/l are presented in Fig. 8. Upstream of the dune, the λ/d_{50} profiles gradually increase with an increase in vertical distance up to $z/h_d \approx 1.25$ and thereafter become almost invariant to the vertical distance, as one goes toward free surface. Downstream of the dune, the λ/d_{50} profiles increase gradually with vertical distance up to $z/h_d \approx 0.75$, and then decrease sharply up to the dune crest. Above the crest, they again start increasing and becoming almost invariant to vertical distance as one goes toward the free surface. It is however evident that at a given z , the Taylor microscale λ in wall-wake flow is smaller than that in undisturbed upstream flow. As the downstream distance increases, the effects of the dune weaken; and far downstream of the dune ($x/l = 3.3$), the λ/d_{50} profiles in both the runs regain their corresponding undisturbed upstream profiles. In conclusion, at a given vertical distance, the length scale of turbulent eddies in the inertial subrange in wall-wake flow is smaller than that in undisturbed upstream flow. The reason is ascribed to an enhanced TKE dissipation rate in wall wake flow.

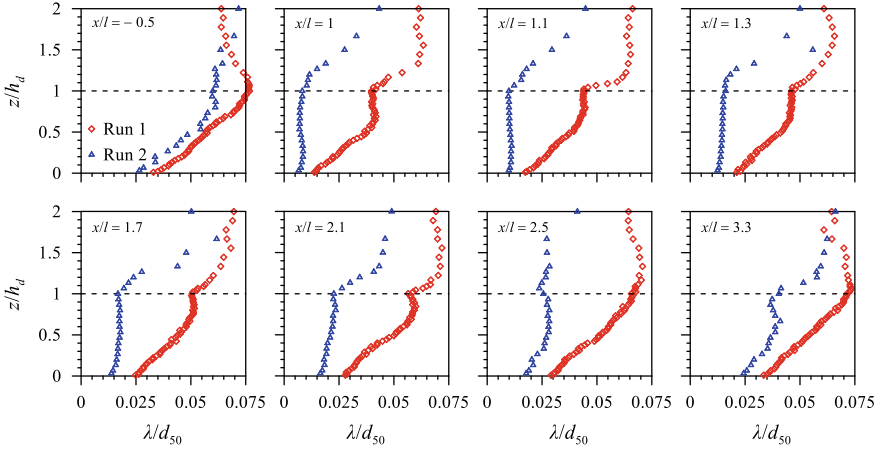


Fig. 8 Vertical profiles of nondimensional Taylor microscale λ/d_{50} at different streamwise distances for Runs 1 and 2

4.3 Kolmogorov Length Scale

In the dissipation range, the viscosity dominates and the TKE is dissipated into heat. The dissipation of TKE takes place at a length scale of the order of the Kolmogorov length scale η , which is expressed as

$$\eta = \left(\frac{\nu^3}{\varepsilon} \right)^{0.25} \quad (3)$$

Figure 9 shows the vertical profiles of nondimensional Kolmogorov length scale η/d_{50} at different nondimensional streamwise distances x/l for Runs 1 and 2. In general, the characteristics of η/d_{50} profiles are almost similar to λ/d_{50} profiles with difference in magnitudes. At a given vertical distance, the Kolmogorov length scale in wall-wake flow is approximately 1/10 times the Taylor microscale.

5 Reynolds Stress Anisotropy

In an *isotropic turbulence*, the velocity fluctuations in a turbulent fluid flow are independent of the axis of reference and invariant to the rotation of axis. It implies the Reynolds normal stresses to be identical, e.g. $\sigma_x = \sigma_y = \sigma_z$, where $(\sigma_x, \sigma_y, \sigma_z) = (\overline{u'u'}, \overline{v'v'}, \overline{w'w'})$. Therefore, the statistics of instantaneous fluid motion at a point correspond to a pure chaotic motion having no preferential direction. On the other hand, in an *anisotropic turbulence*, the velocity fluctuations $u'_i [= (u', v', w')]$ for $i =$

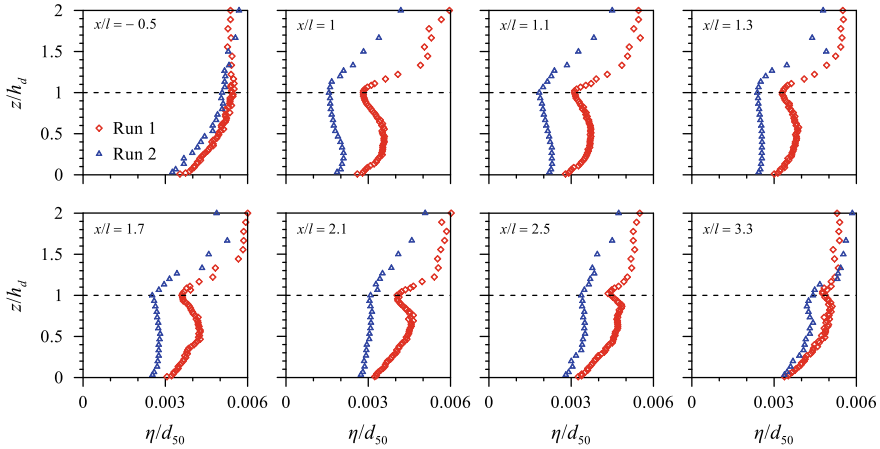


Fig. 9 Vertical profiles of nondimensional Kolmogorov length scale η/d_{50} at different streamwise distances for Runs 1 and 2

(1, 2, 3)] in a turbulent fluid flow are directionally preferred; and hence, the Reynolds normal stresses are not identical.

The Reynolds stress anisotropy remains an important feature in the realm of many natural and industrial flow characteristics, where the notion of isotropic turbulence breaks down. The *Reynolds stress anisotropy tensor* a_{ik} is defined as $a_{ik} = \overline{u'_i u'_k} - (2/3)q\delta_{ik}$ (Rotta 1951), where $q = \overline{u'_i u'_i}/2$ and δ_{ik} is the Kronecker delta function, defined as $\delta_{ik}(i \neq k) = 0$ and $\delta_{ik}(i = k) = 1$. In nondimensional form, the Reynolds stress anisotropy tensor a_{ik} is expressed as $b_{ik} [= a_{ik}/(2q)] = \overline{u'_i u'_k}/(2q) - \delta_{ik}/3$. In essence, the b_{ik} remains a symmetric and traceless tensor ranging from $-1/3$ to $2/3$ and vanishes for an isotropic turbulence ($b_{ik} = 0$). The contribution from the Reynolds stress relative to the TKE corresponds to the sign of each diagonal component in b_{ik} . Figure 10a, b illustrate the vertical profiles of Reynolds stress anisotropy tensor components b_{ik} at different streamwise distances for Runs 1 and 2, respectively. Downstream of the dune, the b_{11} and b_{22} components suggest the wall-wake flow yields less anisotropic turbulence in streamwise direction and more in spanwise direction below the crest. On the other hand, the b_{33} component produces more anisotropic turbulence in the lower half and less in the upper half of the dune, as compared to their undisturbed upstream values. However, the b_{13} component, which signifies the ratio of RSS to TKE, exhibits little change in wall-wake flow. For all b_{ik} components in both the runs, they display a kink at the crest level. However, a recovery is evident, as downstream distance increases.

To portray the degree and the nature of Reynolds stress anisotropy, it is quite convenient to introduce the second and third principal invariants, $I_2 (= -b_{ik}b_{ik}/2)$ and $I_3 (= b_{ij}b_{jk}b_{ki}/3)$, respectively. Since the b_{ik} is a traceless tensor, the first invariant, $I_1 (= b_{ii})$, becomes zero. A quantitative description of total Reynolds stress anisotropy is ascertained by plotting $-I_2$ against I_3 , termed *anisotropy invariant map* (AIM). In an AIM, the feasible turbulence states are confined to the space bounded by the

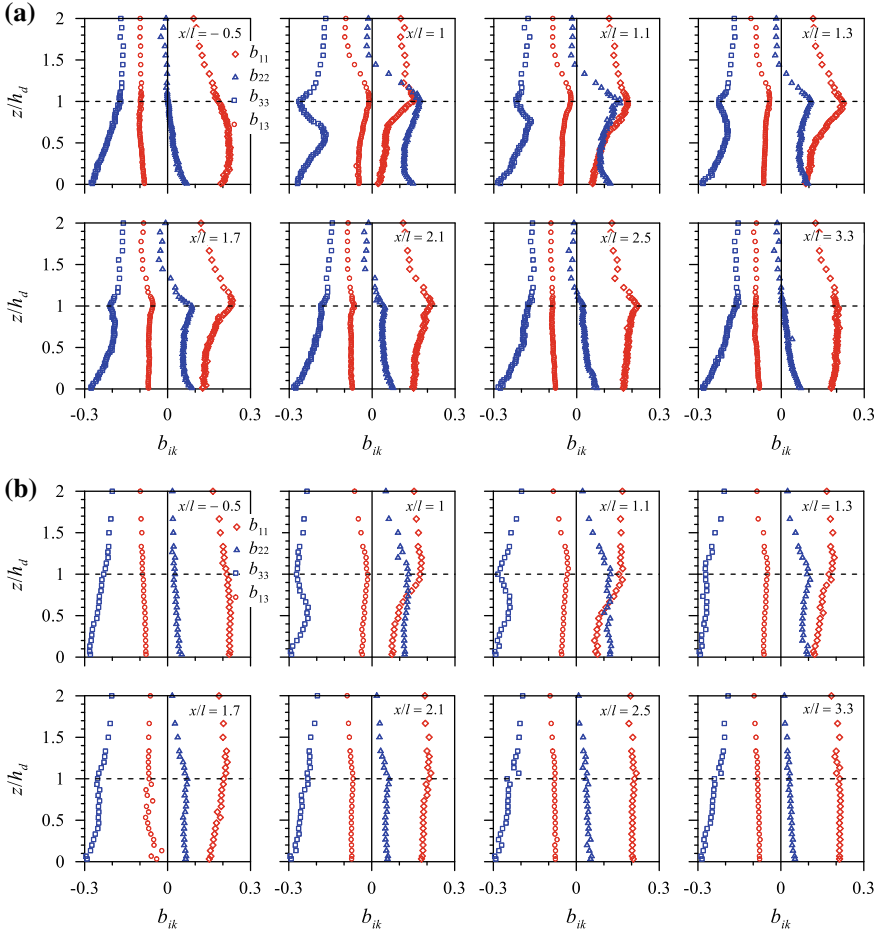


Fig. 10 Vertical profiles of Reynolds stress anisotropy tensor b_{ik} at different streamwise distances for **a** Run 1 and **b** Run 2

left-curved, the right-curved and the top-linear boundaries, forming a triangle, called the *Lumley triangle* (Fig. 11). The left-curved and the right-curved boundaries, being symmetric about the *plane-strain limit* ($I_3 = 0$), evolve from the isotropic limit ($I_2 = I_3 = 0$), obeying a generic relationship as $I_3 = \pm 2(-I_2/3)^{3/2}$. On the other hand, the top-linear boundary follows $I_3 = -(9I_2 + 1)/27$. The current understanding of the states of Reynolds stress anisotropy has so far been achieved on the basis of two different perspectives—the shape of turbulent eddies (Reynolds and Kassinos 1995) and the shape of ellipsoid that the Reynolds stress tensor forms (Simonsen and Krogstad 2005). To be specific, Simonsen and Krogstad (2005) provided a clarification concerning the traditionally used terminologies to describe the states of anisotropy founded on the concept of the shape of turbulent eddies. They concluded